Improved power conversion efficiency for dye-sensitized solar cells using a subwavelength-structured antireflective coating

Chun-Chi Chou, Kuan-Yi Tsao, Chih-Chung Wu, Hongta Yang[*], Chih-Ming Chen[**]

Department of Chemical Engineering, National Chung Hsing University, 250, Kuo Kuang Road, Taichung 402, Taiwan

ABSTRACT

Large-scale, subwavelength-structured nanodome arrays were successfully fabricated using simple, scalable bottom-up colloidal (nanosphere) lithography on a glass substrate as an efficient antireflective photoanode for dye-sensitized solar cells (DSSCs). A self-assembled monolayer of close-packed colloidal crystals (silica) was used as a structural template to pattern the two-dimensional subwavelength-structured nanodome arrays, which function as an efficient antireflective coating due to the graded refractive index across the interface between the air and specific nanodome array structure. The light harvesting for a DSSC with a subwavelength-structured antireflective coating was enhanced due to the improved broadband antireflectivity. Adjusting the nanodome size yielded a short-circuit current density (J_{SC}) of 15.88 mA/cm^2 with a power conversion efficiency (PCE) of 8.82%, which were both better than the reference cell without a subwavelength-structured antireflective coating (J_{SC} = 15.26 mA/cm^2 and PCE = 8.45%).

© 2014 Elsevier B.V. All rights reserved.

1. Introduction

Abundantly available solar energy has long been recognized as an important alternative energy source. Photovoltaic device development plays a crucial role in efficiently converting solar energy into electricity. Dye-sensitized solar cells (DSSCs) have developed into a successful photovoltaic device based on numerous studies over the past two decades [1–5]. However, more effort is needed to meet commercialization requirement such as power conversion efficiency (PCE) comparable to Si-based solar cells, durability for long-term operation, and mass producible assembly technique. Enhancing light utilization in a DSSC is useful for improving the PCE. One common method is to enhance the molar extinction coefficient of the sensitizers (dye molecules) via a specific molecular design or structural modification [6–8]. Co-sensitization using two or more sensitizers [9–11], introducing a scattering medium [12–15], and spectrum down-/up-conversion via Förster resonance energy transfer (FRET) [16,17] are also useful approaches toward efficient light harvesting.

Periodic micro-/nano-structures in biological systems with unique functionalities have provided significant inspiration for practical applications [18–20]. For instance, the corneal sub-300 nm nipple arrays in nocturnal moth eyes reduce reflections over a wide range of wavelengths [21]. This reflection reduction results from a refractive index gradient across the interface between the air and cornea due to the specific nipple array structure [22]. Subwavelength-structured gratings with a smaller period than the wavelength of incident light based on the broadband antireflection properties of moth eyes have been extensively exploited using top-down and bottom-up technologies [23–29]. Subwavelength-structured gratings fabricated on Si substrate exhibited good antireflection performance and thereby improved the light harvesting and photovoltaic performance of Si-based solar cells [30,31]. Unfortunately, the high cost and low throughput of top-down lithography-based fabrication technologies is concerning. Bottom-up self-assembly technologies are inexpensive, simple to implement, and high throughput alternatives to lithography technologies [32–34]. However, most currently available self-assembly technologies involve multiple steps, and are incompatible with fabrication scale-up.

Light reflection suppression by an antireflective coating (ARC) fabricated on a Si substrate using colloidal lithography has been extensively investigated [18–34]; however, applications of such bio-inspired nanostructures to glass substrates is relatively limited [35–38]. Li et al. [35,39] used polystyrene (PS) microspheres as mask in the colloidal lithography process and fabricated an ARC on a silica surface to improve the light transmittance. The best light transmittance for this ARC was in the visible region when

* Corresponding author. Tel.: +886 4 22840510 711; fax: +886 4 22854734.
** Corresponding author. Tel.: +886 4 22840510 511; fax: +886 4 22854734.
E-mail addresses: hyang@dragon.nchu.edu.tw (H. Yang),
chencm@nchu.edu.tw (C.-M. Chen).

the nipple array period was 210 nm [39], whereas a 580 nm period enhanced the light transmittance better in the near-infrared light regions [35]. This period dependence for the ARC allows for a high variety of practical applications. The bio-inspired structure was also applied to the photoanode surface of a DSSC to increase its light transmittance and PCE [40]. However, the moth-eye structure was fabricated by coating an additional polymeric film on the glass substrate using a nanostamp patterning technique. Some material characteristics, for example, the coefficient of thermal expansion (CTE), for the polymer may differ significantly from the glass substrate, which likely causes thermal instability and delamination.

In this study, we developed a simple, inexpensive, and scalable bottom-up colloidal lithography for self-assembling a monolayer of close-packed colloidal crystals (silica) as structural templates for patterning two-dimensional microstructure arrays to mass-fabricate large-scale ARC in a single step. The silica nanospheres became nanodomes after reactive ion etching (RIE) and firmly adhered to the underlying homogeneous glass substrate to form a subwavelength-structured ARC. The nanodome array ARC simultaneously suppressed reflection and enhanced light transmittance over a wide range of wavelengths. Due to the enhanced light transmittance, the incident photon to current efficiency (IPCE) was improved for a DSSC using such a surface-modified electrode, and the PCE of the DSSC improved accordingly.

2. Experimental procedures

2.1. Preparation and characterization of subwavelength-structured antireflective coatings on a glass substrate

The reagents used to synthesize the silica microspheres, including tetraethyl orthosilicate (TEOS, 98%) and ammonium hydroxide (28%), were purchased from Sigma–Aldrich. Ethanol (99.8%) and ethylene glycol (99%) were obtained from ECHO. All of the solvents and chemicals were used without further purification except for TEOS, which was distilled immediately before use. Monodispersed silica particles with various diameters (180, 250, and 315 nm) were synthesized using the standard Stöber method [41]. The synthesized silica microspheres were purified via multiple centrifugation/redispersion cycles in ethanol before redispersing into ethylene glycol. The silica sphere volume fractions for these suspensions were controlled to 0.10. Using a clamp attached to the syringe pump, a fluorine-doped tin oxide (FTO) glass sheet was vertically immersed in a Kimax crystallizing dish containing deionized water. The silica/ethylene glycol suspension was added dropwise to the water surface. The silica spheres rapidly dispersed to form a floating colloidal monolayer at the air/water interface. The glass sheet was then withdrawn at a rate of ~5 cm/min using a KD Scientific 780–230 syringe pump [42,34]. As the glass sheet was withdrawn, the floating colloidal monolayer transferred to both of its sides.

Fig. 1 shows a schematic illustration of the templating procedure for fabricating these subwavelength-structured nipple arrays on a glass sheet. As mentioned above, the colloidal silica sphere monolayers were generated on both sides of the FTO glass sheet. Before the RIE treatment, the colloidal monolayer on the FTO side was wiped off to leave a colloidal monolayer only on the back (illuminated side) of the glass sheet. An oxygen + argon RIE process was then performed on the back (illuminated side) of the glass sheet at 2×10^{-5} Torr and 50 W. The oxygen and argon flow rates were 15 and 5 SCCM, respectively. During the RIE process, the silica particles functioned as an etching mask to protect the glass underneath them from being etched [32], while the non-protected glass surface was etched. After an appropriately long RIE treatment, subwavelength-structured nipple arrays formed on the glass surface as shown in Fig. 1. The surface morphology and cross section of these nipple arrays were examined using scanning electron microscopy (SEM) and atomic force microscopy (AFM). The optical properties of the FTO glass sheet with these subwavelength-structured nipple arrays were also analyzed. The transmittance spectra was measured using a UV–vis spectroscopy (SHIMADZU mini-1240), and the diffuse reflection spectra was measured using a solar cell quantum efficiency QE/IPCE measurement system (Zolix Solar Cell Scan 100) equipped with an integrating sphere and silicon diode detector.

2.2. Assembly and photovoltaic performance of DSSCs based on the antireflective coating

The fabricated FTO glass sheet with subwavelength-structured nipple arrays was used as the substrate to coat a TiO_2 mesoporous film. A 0.16 cm^2 TiO_2 paste coating (Ti-Nanoxide T20/SP, Solaronix) was formed on the FTO side of the glass substrate via screen-printing (ATMA, AT-45PA). After sequentially sintering in an oven at 325 °C for 5 min, 375 °C for 5 min, 450 °C for 15 min, and 500 °C for 15 min, a 9.5 μm thick TiO_2 mesoporous film (7.5 μm nanoparticle layer + 2 μm scattering layer) had formed on the FTO glass substrate as the photoanode. A 1.5 cm × 1.5 cm FTO glass sheet (10 Ω/□,
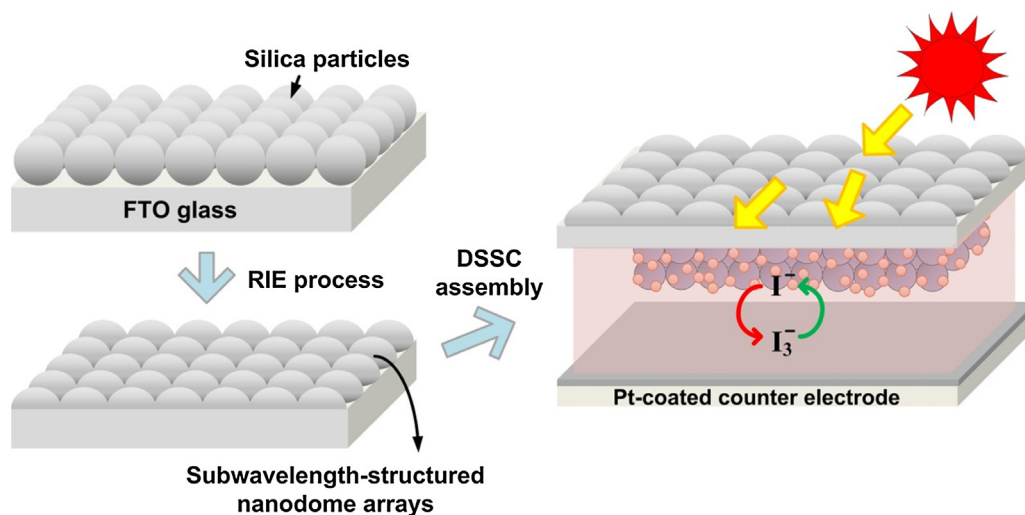

Fig. 1. Schematic illustration of templating procedure for fabricating the subwavelength-structured nanodome arrays on the glass sheet and assembly of DSSCs.
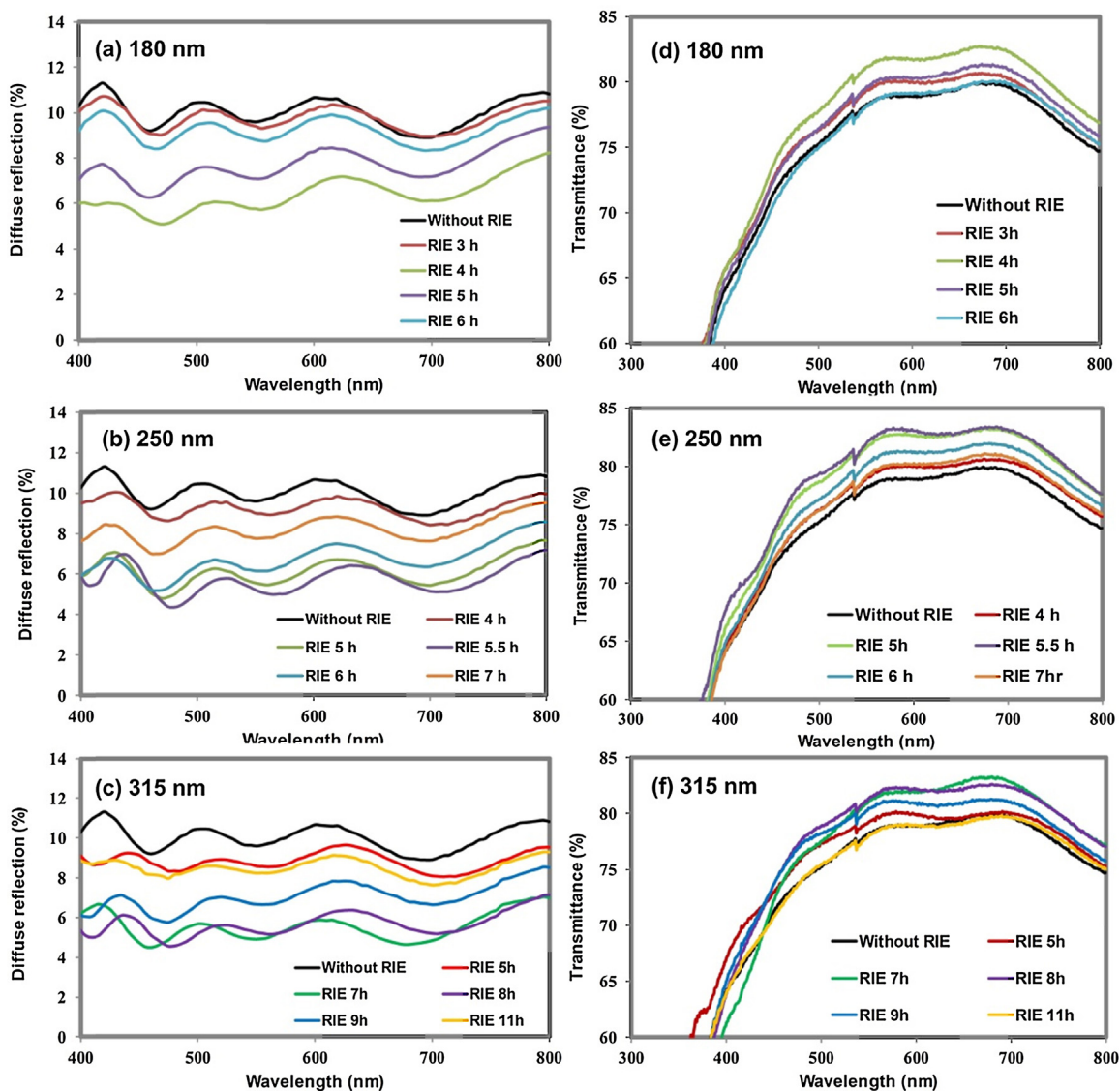
Fig. 2. Optical transmittance and diffuse reflection of glass substrates before and after RIE treatment for various lengths of etching time.

2.2 mm Tripod Technology Corp., Taiwan) was coated with an ultra-thin platinum layer via a solution-based dipping process [43,44] as the counter electrode. The TiO_2-coated photoanode was dipped in a dye solution (0.42 mM N719) for 4 h at room temperature. The photoanode was then assembled with the Pt-coated ITO counter electrode. The appropriate amount of liquid electrolyte (0.1 M LiI, 0.05 M I_2, 0.6 M PMII, 0.5 M TBP, and 0.2 M TBAI in AN/VN 85:15) was injected into the gap between the two electrodes. The as-fabricated DSSC was evaluated under AM 1.5 (1 sun) illumination using a solar simulator (YSS-E40, Yamashita Denso Corp., Japan). The photocurrent–photovoltage (J–V) curves were recorded using a computer-controlled digital source meter (Keithley Model 2400, Keithley Instruments Inc., USA). The IPCE spectrum was measured using a QE/IPCE measurement system (Zolix Solar Cell Scan 100).

3. Results and discussion

3.1. Optical performance of glass substrates with subwavelength-structured ARCs

Three silica particles with different diameters (180, 250, and 315 nm) were monodispersed onto glass substrates and

RIE-treated to fabricate subwavelength-structured ARCs on the glass surface. Various etching times were tested for the three silica particle diameters to optimize the optical performance of the subwavelength-structured ARCs. As shown in Fig. 2, the diffuse reflection was suppressed and the light transmittance was simultaneously enhanced over a wide range of wavelengths for the RIE-treated glass substrates, which indicates the subwavelength-structured ARCs did improve the optical performance of the glass substrate. The best optical performances were achieved at etching times of 4, 5.5, and 8 h for diameters of 180, 250, and 315 nm, respectively. Under these etching and silica size conditions, the resulting ARCs reduced the diffuse reflection to 5–6%, approximately one half that of the glass substrate without an ARC (10%). The best light transmittance was augmented approximately 4–5% relative to the glass substrate without an ARC.

3.2. Microstructural examination of subwavelength-structured ARCs on glass surface

Fig. 3 shows the silica particle microstructures with three diameters coated on the glass surface before and after RIE etching. Before RIE etching, the silica particles, coated using the Langmuir–Blodgett
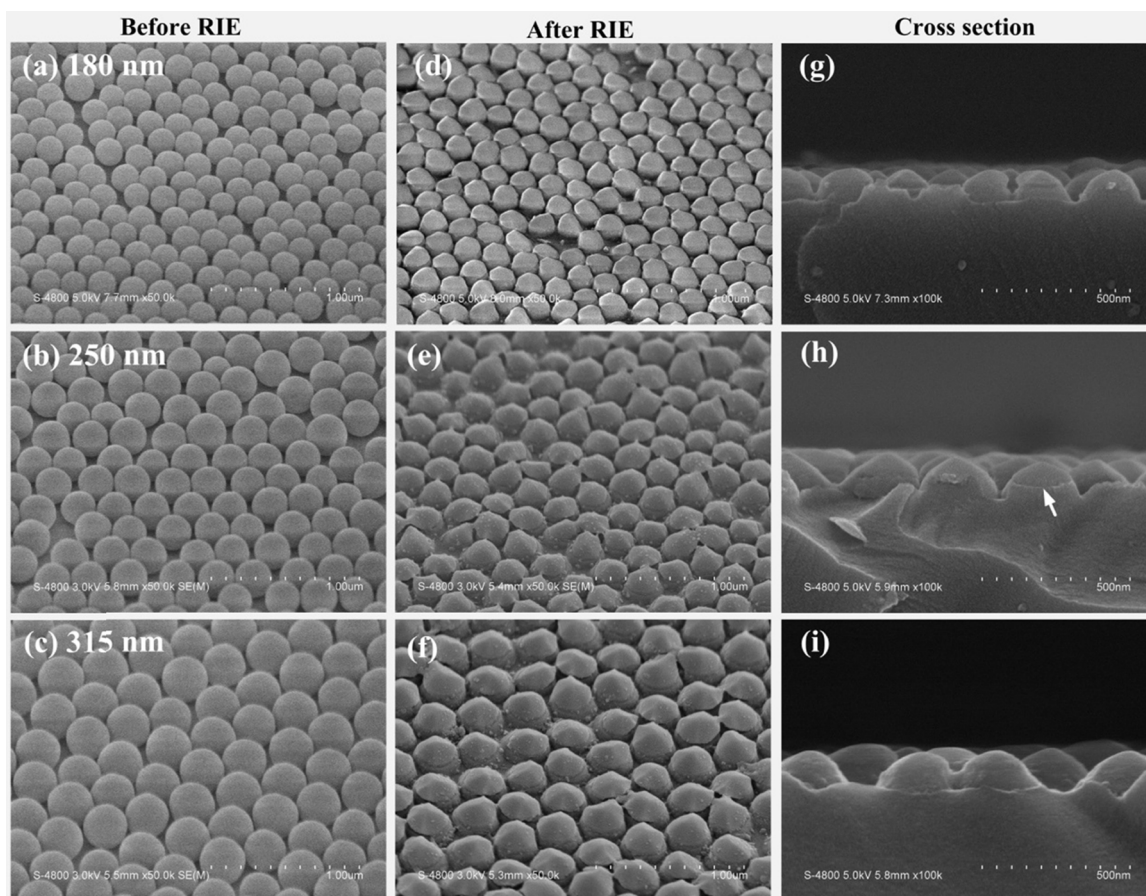
Fig. 3. Top-view SEM images of silica particles with three diameters coated on the glass surface (a)–(c) before and (d)–(f) after RIE etching. (g)–(i) Show the cross-sectional SEM images of subwavelength-structured nanodome arrays.

method [42], were close-packed on the glass surface. These silica particles served as an etching mask protecting the glass underneath. The reactive ions etched the uncovered glass surface, which caused the protected glass surface to protrude and gradually formed the subwavelength-structured nanodome arrays shown in Fig. 3(d)–(f) for the 180, 250, and 315 nm samples, respectively. The etching times were 4, 5.5, and 8 h for 180, 250, and 315 nm, respectively, which were the times with the best optical performance as mentioned above. Fig. 3(g)–(i) shows cross sections of the nanodome arrays on the glass surface. Each nanodome was constructed with a cap adhering above a trapezoid with a visible boundary between them as shown by the arrow in Fig. 3(h). The cap evolved from the silica particle and the trapezoid formed from the base glass substrate during the RIE treatment. Severe scratching with sandpaper had difficulty removing the cap from the base trapezoid, which indicates a strong adhesion between the cap and trapezoid. The nanodome sizes were reduced from those of original silica particle, and all nanodomes exhibited a longer base width with a shorter height as shown in Table 1. The nanodome array periods were approximately 199, 260, and 305 nm for the 180, 250,

and 315 samples, respectively, based on the cross-sectional AFM images shown in Fig. 4. All of the periods were sufficiently small to enhance the light transmittance over a broad range of wavelengths. The root-mean-square roughness (R_{rms}) was the lowest (1.19 nm) for a glass surface without any structural modification, while the R_{rms} increased to 16.75, 24.87, and 29.70 nm for the 180, 250, and 315 nm samples, respectively.

3.3. Photovoltaic performance for DSSCs using the antireflective coatings

Fig. 5 shows J–V curves representative of the DSSCs fabricated with and without a subwavelength-structured ARC. The V_{OC} was similar for all of the DSSCs; however, the J_{SC} was improved in the DSSCs with an ARC (type 180, 250, and 315) over that without an ARC (reference cell). To statistically investigate the effects of the ARC, at least five cells were fabricated for each type of DSSC, and their J–V curves were measured. Table 2 lists the average photovoltaic characteristics for the DSSCs determined from their J–V curves. DSSCs without a subwavelength-structured ARC (reference

Table 1
Dimensions of nanodome arrays in subwavelength-structured antireflective coatings.

	Silica size		
	180 nm	250 nm	315 nm
Height (nm)	108	138	149
Base width (nm)	178	234	278
Period (nm)	199	260	305

Table 2
Photovoltaic characteristics of DSSCs with and without a subwavelength-structured antireflective coating.

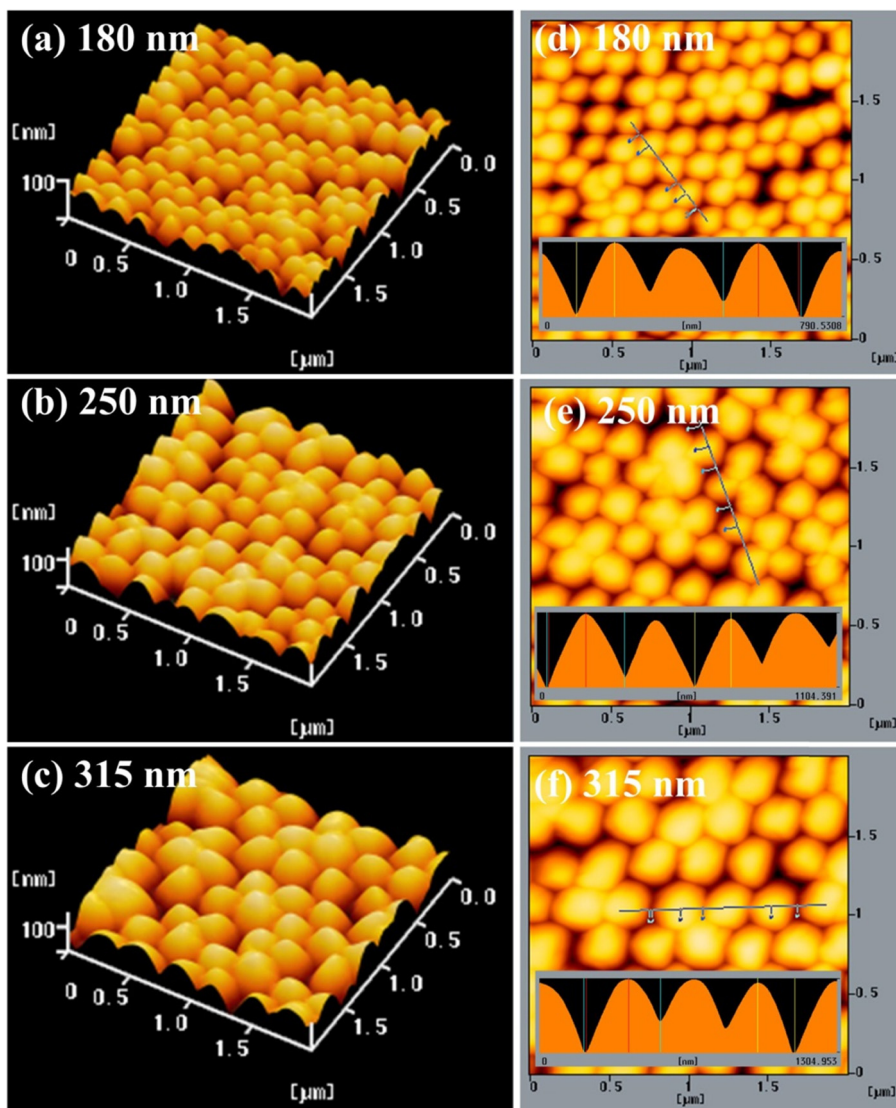| Type	J_{SC} (mA/cm^2)	V_{OC} (V)	FF	PCE (%)
Reference cell	15.26	0.757	0.731	8.45
Type 180	15.57	0.759	0.731	8.64
Type 250	15.78	0.759	0.726	8.70
Type 315	15.88	0.759	0.731	8.82

Fig. 4. AFM images of subwavelength-structured nanodome arrays coated on the glass surface: (a)–(c) side view, (d)–(f) top view and the insets show cross-sectional view.

cell) exhibited a PCE of 8.45% with the following photovoltaic parameters: J_{SC} = 15.26 A/cm^2, V_{OC} = 0.757 V, and FF = 0.731. In contrast, the PCE improved for DSSCs with subwavelength-structured ARCs, which was apparently due to the improved J_{SC}. The best J_{SC}

obtained was 15.88 mA/cm^2 for the 315 nm DSSC, and the resulting PCE reached 8.82%, which was the highest for all of the tested cells. This result indicated the subwavelength-structured ARC enhanced the photoanode light transmittance (as confirmed in Fig. 2), which increased the incident light harvested by the N719 dye molecules
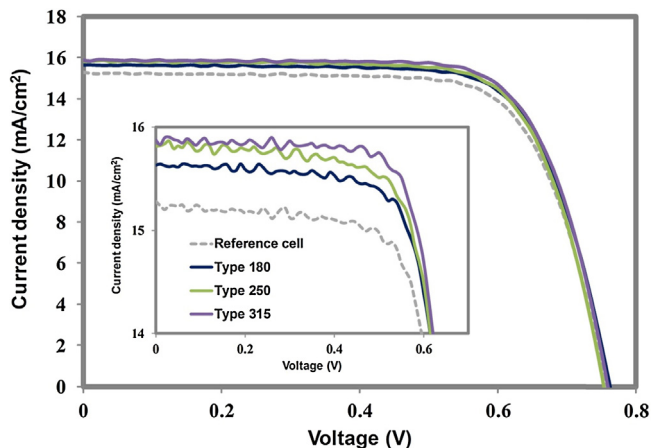

Fig. 5. Representative photocurrent–photovoltage (J–V) curves of DSSCs fabricated with (type 180, 250, and 315) and without (reference) a subwavelength-structured antireflective coating.
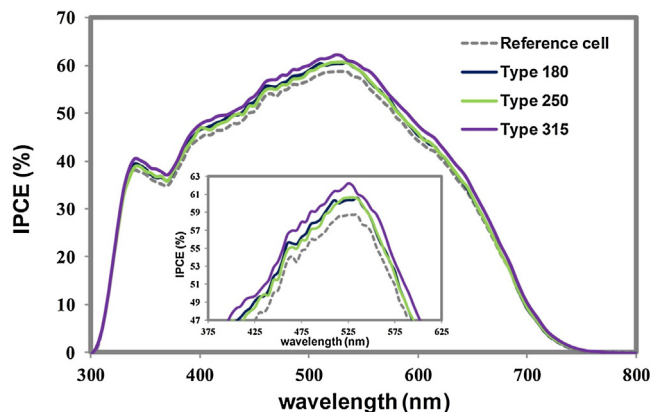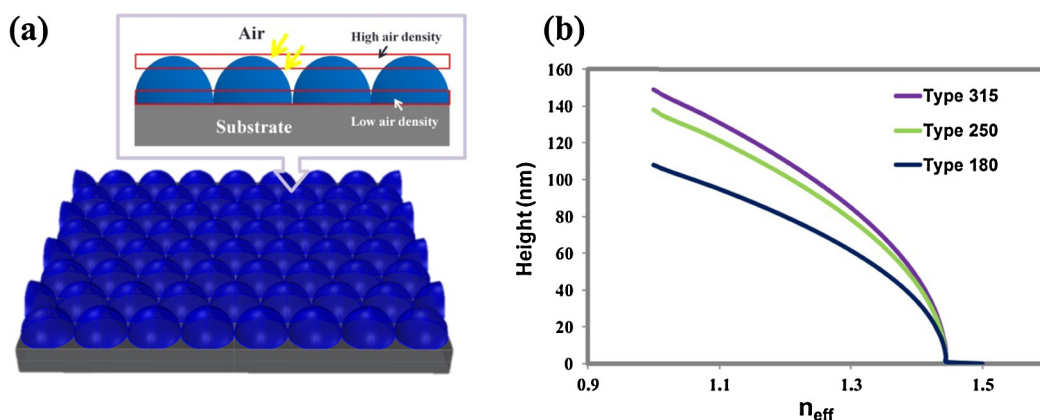

Fig. 6. IPCE spectra of DSSCs fabricated with (type 180, 250, and 315) and without (reference) a subwavelength-structured antireflective coating.

Fig. 7. (a) Illustration of subwavelength-structured nanodome arrays arranged in a close-packed order on the glass surface. (b) Effective refractive index (n_{eff}) as a function of height of nanodome fabricated on glass surface.

and thus the PCE. Fig. 6 shows the IPCE spectra for the four types of DSSCs, and those based on subwavelength-structured ARC (type 180, 250, and 315) exhibited better IPCE performance over the visible wavelength range than those without an ARC (reference cell). These results confirmed the incident light harvested by the N719 dye molecules was indeed enhanced by the ARC. The exterior ARC did not affect the energy bandgap relationship between the TiO_2 and electrolyte within the DSSC; therefore, the V_{OC} was similar between the DSSCs with and without an ARC. Similarly, the FF variation was insignificant for all of the tested DSSCs because the exterior ARC did not affect the electron transport properties and impedance within the DSSC.

The enhanced light transmittance using a subwavelength-structured ARC was attributed to a refractive index gradient across the interface between the air and nanodome array. These specific nanodome arrays effectively suppressed reflection by gradually reducing the effective refractive index away from the glass substrate surface, which enhanced the light transmittance [45]. The effective refractive index (n_{eff}) can be determined by averaging the refractive indices for air and glass (SiO_2) weighted by the volume at their interface as expressed by the following simulation [45].

$$n_{eff} = V_{air}(\%) \times n_{air} + V_{SiO_2}(\%) \times n_{SiO_2} \qquad (1)$$

where V_{air} and V_{SiO_2} are the volume fractions for air and SiO_2 (glass), respectively, and n_{air} and n_{SiO_2} are the refractive indices for air and SiO_2 (glass), respectively, and are 1 and 1.5, respectively. At the top of the nanodome arrays, V_{air} is nearly 100% and V_{SiO_2} is nearly zero, so the n_{eff} is close to n_{air}. However, V_{air} decreases while V_{SiO_2} increases upon approaching to the nanodome array base. Thus, n_{eff} nearly equals n_{SiO_2} at the nanodome array base. To calculate the effective refractive index for the ARC, we assumed all of the subwavelength-structured nanodome arrays were semi-ellipses arranged in a close-packed order on the glass surface as illustrated in Fig. 7(a). The dimensions (base width and height) for the 180, 250, and 315 nm semi-ellipses were set to those listed in Table 1. Using the widths and heights for the semi-ellipses in Eq. (1) allows n_{eff} to be calculated as a function of the semi-ellipse height as shown in Fig. 7(b). The n_{eff} gradually changed from 1 (n_{air}) to 1.5 (n_{SiO_2}) upon reducing the semi-ellipse height for all three sizes (180, 250, and 315). The 315 nm samples exhibited the best antireflective performance because the n_{eff} transition from $n = 1$ for air to $n = 1.5$ for glass (SiO_2) with increasing depth was the smoothest. This result indicates the subwavelength nanostructure height plays a crucial role, that is, the larger the height, the more gradual the refractive index changes, which decreases the light reflection [40]. These findings were consistent with the IPCE spectra results (Fig. 6) where

the 315 nm DSSC exhibited the best light harvesting performance. Therefore, the 315 nm DSSC exhibited the best J_{SC} and PCE.

4. Conclusions

A bottom-up colloidal lithography with self-assembled close-packed silica nanospheres (180, 250, and 315 nm) as structural templates was used to fabricate an efficient ARC onto the illuminated side of DSSCs. This anti-reflective coating consisted of subwavelength-structured nanodome arrays that effectively suppressed light reflection via a graded refractive index across the interface between the air and nanodomes. The diffuse reflection was reduced to 5–6%, which was approximately one half of the glass substrate without an anti-reflective coating (10%). The light transmittance was enhanced 4–5% on the illuminated side for the DSSCs, and the IPCE and short-circuit current density both improved accordingly. Depending on the nanodome array height, the short-circuit current density was enhanced from 15.57 to 15.88 mA/cm^2 relative to the reference cell without a subwavelength-structured anti-reflective coating (15.26 mA/cm^2). The power conversion efficiency was enhanced from 8.45% (reference cell) to 8.64–8.82% using the subwavelength-structured anti-reflective coating. The DSSC power conversion efficiency can be enhanced further by minimizing the light reflection loss by optimizing the anti-reflective coating profile by increasing the nanodome height or accurately controlling the nanodome aspect ratio to form pillar-like nanostructures under different etching conditions.

References

[1] B. O'Regan, M. Grätzel, A low-cost, high-efficiency solar cell based on dye-sensitized colloidal TiO_2 films, Nature 353 (1991) 737–740.

[2] M. Grätzel, Photoelectrochemical cells, Nature 414 (2001) 338–344.

[3] P. Péchy, T. Renouard, S.M. Zakeeruddin, R. Humphry-Baker, P. Comte, P. Liska, L. Cevey, E. Costa, V. Shklover, L. Spiccia, G.B. Deacon, C.A. Bignozzi, M. Grätzel, Engineering of efficient panchromatic sensitizers for nanocrystalline TiO_2-based solar cells, J. Am. Chem. Soc. 123 (2001) 1613–1624.

[4] S. Mathew, A. Yella, P. Gao, R. Humphry-Baker, B.F.E. Curchod, N. Ashari-Astani, I. Tavernelli, U. Rothlisberger, M.K. Nazeeruddin, M. Grätzel, Dye-sensitized solar cells with 13% efficiency achieved through the molecular engineering of porphyrin sensitizers, Nat. Chem. 6 (2014) 242–247.

[5] T.Y. Tsai, C.M. Chen, S.J. Cherng, S.Y. Suen, An efficient titanium-based photoanode for dye-sensitized solar cell under back-side illumination, Prog. Photovolt. Res. Appl. 21 (2013) 226–231.

[6] S. Ito, H. Miura, S. Uchida, M. Takata, K. Sumioka, P. Liska, P. Comte, P. Péchy, M. Grätzel, High-conversion-efficiency organic dye-sensitized solar cells with a novel indoline dye, Chem. Commun. (2008) 5194–5196.

[7] C.Y. Chen, S.J. Wu, J.Y. Li, C.G. Wu, J.G. Chen, K.C. Ho, A new route to enhance the light-harvesting capability of ruthenium complexes for dye-sensitized solar cells, Adv. Mater. 19 (2007) 3888–3891.

[8] C.Y. Chen, J.G. Chen, S.J. Wu, J.Y. Li, C.G. Wu, K.C. Ho, Multifunctionalized ruthenium-based supersensitizers for highly efficient dye-sensitized solar cells, Angew. Chem. Int. Ed. 47 (2008) 7342–7345.

[9] A. Yella, H.W. Lee, H.N. Tsao, C. Yi, A.K. Chandiran, M.K. Nazeeruddin, E.W.G. Diau, C.Y. Yeh, S.M. Zakeeruddin, M. Grätzel, Porphyrin-sensitized solar cells with cobalt (II/III)-based redox electrolyte exceed 12 percent efficiency, Science 334 (2011) 629–634.

[10] P.J. Holliman, K.J. Al-Salihi, A. Connell, M.L. Davies, E.W. Jonesa, D.A. Worsley, Development of selective, ultra-fast multiple co-sensitization to control dye loading in dye-sensitized solar cells, RSC Adv. 4 (2014) 2515–2522.

[11] F. Huang, D. Chen, L. Cao, R.A. Caruso, Y.B. Cheng, Flexible dye-sensitized solar cells containing multiple dyes in discrete layers, Energy Environ. Sci. 4 (2011) 2803–2806.

[12] M. Ye, C. Chen, M. Lv, D. Zheng, W. Guo, C. Lin, Facile and effective synthesis of hierarchical TiO_2 spheres for efficient dye-sensitized solar cells, Nanoscale 5 (2013) 6577–6583.

[13] X. Miao, K. Pan, Y. Liao, W. Zhou, Q. Pan, G. Tian, G. Wang, Controlled synthesis of mesoporous anatase TiO_2 microspheres as a scattering layer to enhance the photoelectrical conversion efficiency, J. Mater. Chem. A 1 (2013) 9853–9861.

[14] K. Zhu, N.R. Neale, A. Miedaner, A.J. Frank, Enhanced charge-collection efficiencies and light scattering in dye-sensitized solar cells using oriented TiO_2 nanotubes arrays, Nano Lett. 7 (2007) 69–74.

[15] D. Chen, F. Huang, Y.-B. Cheng, R.A. Caruso, Mesoporous anatase TiO_2 beads with high surface areas and controllable pore sizes: a superior candidate for high-performance dye-sensitized solar cells, Adv. Mater. 21 (2009) 2206–2210.

[16] J. Liu, Q. Yao, Y. Li, Effects of downconversion luminescent film in dye-sensitized solar cells, Appl. Phys. Lett. 88 (2006) 173119.

[17] Y.J. Lin, C.C. Chang, S.J. Cherng, J.W. Chen, C.M. Chen, Manipulation of light harvesting for efficient dye sensitized solar cell by doping an ultraviolet light capturing fluorophore, Prog. Photovolt. Res. Appl. (2013), http://dx.doi.org/10.1002/pip.2407.

[18] P. Vukusic, J.R. Sambles, Photonic structures in biology, Nature 424 (2003) 852–855.

[19] M. Sirnivasarao, Nano-optics in the biological world: beetles, butterflies, birds, and moths, Chem. Rev. 99 (1999) 1935–1961.

[20] J. Aizenberg, D.A. Muller, J.L. Grazul, D.R. Hamann, Direct fabrication of large micropatterned single crystals, Science 299 (2003) 1205–1208.

[21] P.B. Clapham, M.C. Hutley, Reduction of lens reflexion by the "moth eye" principle, Nature 244 (1973) 281–282.

[22] W.L. Min, A.P. Betancourt, P. Jiang, B. Jiang, Bioinspired broadband antireflection coatings on GaSb, Appl. Phys. Lett. 92 (2008) 141109.

[23] Y. Kanamori, M. Sasaki, K. Hana, Broadband antireflection graftings fabricated upon silicon substrates, Opt. Lett. 24 (2009) 2476–2482.

[24] K.M. Baker, Highly corrected close-packed microlens arrays and moth-eye structuring on curved surfaces, Appl. Opt. 38 (1999) 352–356.

[25] Q. Chen, G. Hubbard, P.A. Shields, C. Liu, D.W.E. Allsopp, W.N. Wang, S. Abbott, Broadband moth-eye antireflection coatings fabricated by low-cost nanoimprinting, Appl. Phys. Lett. 94 (2009) 2631–2718.

[26] C. Heine, R.H. Morf, Submicrometer graftings for solar energy applications, Appl. Opt. 34 (1999) 2476–2482.

[27] Y. Zhao, J.S. Wang, G.Z. Mao, Colloidal subwavelength nanostructures for antireflection optical coatings, Opt. Lett. 30 (2005) 1885–1887.

[28] B.G. Prevo, E.W. Hon, O.D. Velev, Assembly and characterization of colloid-based antireflective coatings on multicrystalline solar cells, J. Mater. Chem. 17 (2007) 791–799.

[29] H. Jiang, K. Yu, Y.C. Wang, Antireflective structures via spin casting of polymer latex, Opt. Lett. 32 (2007) 575–577.

[30] H. Sai, H. Fujii, K. Arafune, Y. Ohshita, Y. Kanamori, H. Yugami, M. Yamaguchi, Wide-angle antireflection effect of subwavelength structures for solar cells, Jpn. J. Appl. Phys. 46 (2007) 3333–3336.

[31] Y.M. Song, J.S. Yu, Y.T. Lee, Antireflective submicrometer gratings on thin-film silicon solar cells for light-absorption enhancement, Opt. Lett. 35 (2010) 276–278.

[32] W.L. Min, B. Jiang, P. Jiang, Bioinspired self-cleaning antireflection coatings, Adv. Mater. 20 (2008) 3914–3918.

[33] K. Asker, B.M. Phillips, Y. Fang, B. Choi, N. Gozubenli, P. Jiang, B. Jiang, Self-assembled self-cleaning broadband anti-reflection coatings, Colloids Surf. A 439 (2013) 84–100.

[34] K. Askar, B.M. Phillips, X. Dou, J. Lopez, C. Smith, B. Jiang, P. Jiang, Self-assembled nanoparticle antiglare coatings, Opt. Lett. 37 (2012) 4380–4382.

[35] Y. Li, J. Zhang, S. Zhu, H. Dong, F. Jia, Z. Wang, Y. Tang, L. Zhang, S. Zhang, B. Yang, Bioinspired silica surfaces with near-infrared improved transmittance and superhydrophobicity by colloidal lithography, Langmuir 26 (2010) 9842–9847.

[36] S. Ji, K. Song, T.B. Nguyen, N. Kim, H. Lim, Optimal moth eye nanostructure array on transparent glass towards broadband antireflection, ACS Appl. Mater. Interfaces 5 (2013) 10731–10737.

[37] F. Tao, P. Hiralal, L. Ren, Y. Wang, Q. Dai, G.A. Amaratunga, H. Zhou, Tuning the peak position of subwavelength silica nanosphere broadband antireflection coatings, Nanoscale Res. Lett. 9 (2014) 361.

[38] Y.M. Song, Y. Jeong, C.I. Yeo, Y.T. Lee, Enhanced power generation in concentrated photovoltaics using broadband antireflective coverglasses with moth eye structures, Opt. Express 20 (2012) A916–A923.

[39] Y. Li, J. Zhang, S. Zhu, H. Dong, F. Jia, Z. Wang, Z. Sun, L. Zhang, Y. Li, H. Li, W. Xu, B. Yang, Biomimetic surfaces for high-performance optics, Adv. Mater. 21 (2009) 4731–4734.

[40] S.Y. Heo, J.K. Koh, G. Kang, S.H. Ahn, W.S. Chi, K. Kim, J.H. Kim, Bifunctional moth-eye nanopatterned dye-sensitized solar cells: light-harvesting and self-cleaning effects, Adv. Energy Mater. 4 (2014) 1300–1632.

[41] W. Stöber, A. Fink, Controlled growth of monodisperse silica spheres in the micron size range, J. Colloid Interface Sci. 26 (1968) 62–69.

[42] A. Ulman, An Introduction to Ultrathin Organic Films: From Langmuir–Blodgett to Self-Assembly, Academic Press, San Diego, 1991.

[43] T.C. Wei, C.C. Wan, Y.Y. Wang, Poly(N-vinyl-2-pyrrolidone)-capped platinum nanoclusters on indium-tin oxide glass as counterelectrode for dye-sensitized solar cells, Appl. Phys. Lett. 88 (2006) 1031–1122.

[44] T.C. Wei, C.C. Wan, Y.Y. Wang, C.M. Chen, H.S. Shiu, Immobilization of poly(N-vinyl-2-pyrrolidone)-capped platinum nanoclusters on indium–tin oxide glass and its application in dye-sensitized solar cells, J. Phys. Chem. C 111 (2007) 4847–4853.

[45] D.G. Stavenga, S. Foletti, G. Palasantzas, K. Arikawa, Light on the moth-eye corneal nipple array of butterflies, Proc. R. Soc. B 273 (2006) 661–667.